Journal of Materials Chemistry A

ROYAL SOCIETY OF CHEMISTRY

PAPER

View Article Online
View Journal

Cite this: DOI: 10.1039/d5ta08956e

Shape-change programming of zwitterionic hydrogels *via* chemical gradients directed by surface energy

Negin Bouzari,[a] Micahel Ali,[b] Edward Hong,[b] Nrushanth Suthaharan,[b] Melanie Bouzanne,[b] Amirreza Aghakhani[c] and Hamed Shahsavan *[a]

Received 4th November 2025
Accepted 30th December 2025

DOI: 10.1039/d5ta08956e

rsc.li/materials-a

Introducing anisotropic swelling to stimuli-responsive hydrogels promises a host of opportunities for their shape-change programming and utility in soft robotic applications. Here, we report a straightforward yet robust method of creating differential swelling within pH-responsive self-healing hydrogels to program their shape-change and mode of deformation. Our strategy relies on a large disparity between the polarity of constituent zwitterionic and non-zwitterionic monomers, which facilitates their deterministic separation and migration toward confining surfaces of different surface energies. Using this method, we obtained hydrogels with a large gradient of chemical formulation across the thickness, capable of controlled and rapid bending upon exposure to a change in environmental pH. We localized such chemical gradients across the hydrogel thickness in-plane by patterning confining substrates with areas of high and low surface energy. Thanks to this strategy and the self-healing properties of our hydrogels, we achieved deformation of two-dimensional hydrogel films to complex three-dimensional structures. The proposed shape-change programming strategy offers a simple yet robust method to produce programmable actuators that are useful in soft aquatic robotic applications.

[a]*Department of Chemical Engineering, Waterloo Institute for Polymer Research, Waterloo Institute for Nanotechnology, Centre for Bioengineering and Biotechnology, University of Waterloo, Waterloo, ON N2L 3G1, Canada. E-mail: hshahsav@uwaterloo.ca*

[b]*Department of Chemical Engineering, University of Waterloo, Waterloo, ON N2L 3G1, Canada*

[c]*Institute of Biomaterials and Biomolecular Systems (IBBS), University of Stuttgart, Pfaffenwaldring 57, Stuttgart 70569, Germany*

Hamed Shahsavan

Hamed Shahsavan has been an assistant professor in the Department of Chemical Engineering at the University of Waterloo since 2020. He obtained his PhD from the University of Waterloo in 2017. He conducted his postdoctoral research as an NSERC fellow at the Max Planck Institute for Intelligent Systems and focused on the application of liquid crystalline elastomers and hydrogels as shape-change programmable materials in soft robots and devices at the millimeter to micrometer scale. His current research interests revolve around a variety of soft, stimuli-responsive, and programmable polymers and different fabrication methods for manufacturing small-scale mobile robots.

Introduction

Hydrogels' remarkable swelling/deswelling properties, which result in their tunable water content and mechanical properties, enable the creation of constructs that closely resemble biological tissues, providing safer interactions with humans.[1–3] Hydrogels have found widespread use in soft robotic structures as they offer enhanced control over their functions and degrees of freedom.[4–10] Responsive hydrogels are capable of transducing external stimuli into structural changes that manifest as mechanical deformation to perform functions such as physical work *via* geometrical expansion and contraction.[3,11–16] These shape changes are typically uncontrolled and isotropic,[17–20] and their spatiotemporal control can lead to more deterministic actions desirable for robotic applications.[21–23]

Shape-change programming of hydrogels is often rooted in their ability to undergo differential swelling, which can be achieved by imparting anisotropic properties into their micro- and macrostructure.[23–27] When exposed to external stimulation, hydrogels under differential swelling experience a buildup of internal stress and elastic energy. To minimize this energy, they deform *via* either buckling or bending, or a combination of both mechanisms, leading to the transformation of a two-dimensional (2D) or three-dimensional (3D) geometry to another.[28,29] The structural anisotropy leading to differential swelling of hydrogels can be achieved at both macro- and microscales.[30]

At the macroscale, structural anisotropy for shape-change programming can be achieved through the hybridization or tessellation of different hydrogels with each other. Hydrogels with different physicochemical properties are integrated into heterolithic structures, and their different swelling behaviour leads to a macroscale differential swelling of the whole construct.[26] At the microscale, one can induce anisotropy by creating gradients in physicochemical properties and morphology of monolithic hydrogels either in-plane or across their thickness. Examples of such strategies include grayscale lithography,[31,32] directional freezing,[33] shear-induced alignment,[34] and voxel-by-voxel programming using two-photon polymerization.[35] Although these methods provide high spatial resolution for shape programming of hydrogels, they often rely on sophisticated equipment and are not readily achievable. Compared to creating microstructural anisotropy in monolithic structures, hybridization and tessellation are more accessible and can be achieved more readily *via* manual stitching, extrusion, and light-based 3D printing.[36–38] However, constructs created through hybridization experience significant shear forces at the interfaces between dissimilar layers during deformation, adversely affecting their mechanical properties and durability.[39–41] Achieving shape-change programming within monolithic hydrogels bypasses such drawbacks of hybridization and tessellation. However, it still poses many technical challenges, especially at larger scales and when more accessible and less expensive programming techniques are preferred.

In this work, we introduce a straightforward yet robust strategy for shape-change programming of monolithic hydrogels made of zwitterionic copolymers. This strategy is based on the large disparity between the polarity of zwitterionic and non-zwitterionic comonomers within a hydrogel precursor. Confining such precursors to substrates with significantly different surface energies before polymerization facilitates monomers' preferential migration. Polymerization of precursors after such migration leads to monolithic hydrogel structures with a gradient in physicochemical properties across the thickness.[42–45] Using this method, and leveraging the self-healing properties of zwitterionic moieties, we demonstrate rapid shape changes with varying levels of complexity by tailoring the hydrogels' geometry. The proposed method presents a versatile strategy that can be applied to hydrogel or polymer blend systems containing molecules with different polarities, thereby expanding the portfolio of shape-change programming techniques pertinent to materials science and soft robotics.

Results and discussion

Concept

Fig. 1a shows the chemicals used in the formulation of our hydrogel precursors. Generally, our hydrogels contain two monomers with significantly different polarities and charge characters: 3-dimethyl (methacryloyloxyethyl) ammonium propanesulfonate (DMAPS), a zwitterionic monomer with high polarity (effective dipole moment of m ~31.82 debye) that forms

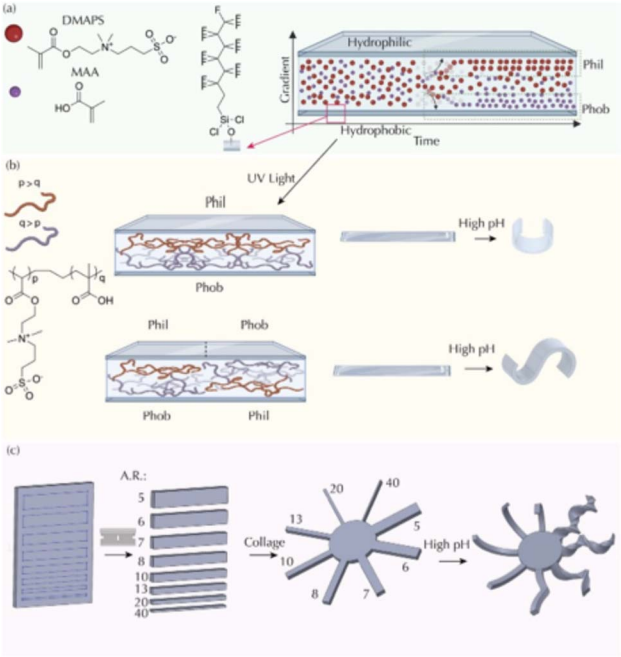

Fig. 1 System concept. (a) The chemical structure of the hydrogel components. DMAPS stands for 3-dimethyl (methacryloyloxyethyl) ammonium propanesulfonate and MAA stands for methacrylic acid. The schematic shows silanization of the glass slide with Trichloro(1*H*,1*H*,2*H*,2*H*-perfluorooctyl) silane as a hydrophobic modification. (b) Schematic representation of the single-domain and multi-domain shape-change programming method used in this study. For single-domain programming, whole glass slides that were in contact to the hydrogel precursor were modified, whereas for multi-domain programming, glass slides were selectively patterned with hydrophobic and hydrophilic areas. (c) Schematic representation of using the cut-and-paste strategy to achieve complex shape-change programming. The schematic shows single-domain gradgels with different aspect ratios attached into a hydrogel circular body by using the cut-and-paste technique. The collaged structure, which resembles an octopus, moves forward at high pH, thanks to the rapid bending and twisting deformation of the legs.

softer hydrophilic polymers ($G' \approx 700$ Pa), and methacrylic acid (MAA), a monomer with less polarity (effective dipole moment of m ~3.42 debye) that forms stiffer polymers with less hydrophilicity.[46–48] Such differences in the mechanical properties of the two gels are related to the difference in their microporous structure, *i.e.*, DMAPS gels have a larger average pore size compared to MAA gels (see Fig. S1). Therefore, at equal sample volumes, DMAPS gels have less mass and swell more, which renders them softer. Each of these co-monomers plays a crucial role in tuning the final composition and behaviour of hydrogels. DMAPS is a zwitterionic molecule having both positive and negative charged groups in its structure. The electrostatic interactions between oppositely charged groups in the zwitterionic polymers and hydrogels of DMAPS provide them with intrinsic self-adhesion or self-healing properties[48] that can be leveraged for the fabrication of shape-change programmed heterolytic structures *via* a cut-and-paste strategy. MAA is responsive to the changes in environmental pH, with an acid dissociation constant of (pK_a) 4.6.[34] When the pH of the

environment exceeds 4.6, the carboxylic acid groups in MAA deprotonate, and the $-COO^-$ groups repel each other. Lowering the pH reverses this process.[49] When incorporated into a hydrogel network, MAA will have similar responsiveness to pH alterations, and its deprotonation leads to excessive hydrogel swelling, water uptake, and, essentially, transduction of chemical energy to mechanical energy. Additionally, a very small amount of *N*, *N*′-bis methylenacrylamide (BIS) was added to the percussor as a chemical cross-linker to enhance the mechanical integrity of the hydrogel samples. We used cellulose nanocrystals (CNC) to tune the mechanical properties and swelling, and shape-change behavior of final hydrogels. Our materials system exhibits high self-healing efficiency, which ensures robust inter-layer adhesion for creating collaged structures with the integrity required for practical applications. The fundamental properties of this system have been thoroughly and systematically investigated in our prior publications. The compositions of all tested precursors are summarized in Table S1. Later, we will discuss the criteria we chose to select a formulation for the rest of our studies.

To achieve the migration of DMAPS and MAA monomers to substrates with higher affinity toward them and create a gradient of composition across the hydrogel, we injected the precursor into capillary cells of known thickness made from hydrophilic and hydrophobic glass slides facing each other (see Fig. S2 in SI). For hydrophilic modification, clean glass slides were put into a UV-Ozone chamber and treated for 30 minutes at room temperature. Liquid phase silanization was used to make hydrophobic glass slides, where clean glass slides were submerged in a solution of Trichloro(1*H*,1*H*,2*H*,2*H*-perfluorooctyl)silane in toluene, and they remained in the solution for two hours inside a fume hood. The precursor was not disturbed for one hour, after which it underwent photopolymerization for another hour. Filled cells were flipped once halfway through the polymerization process. During this process, we expected that the resulting gradient of monomers across the thickness would be frozen-in within hydrogels where copolymer chains grow with different numbers of DMAPS (p) and MAA (q). Hereafter, we refer to such hydrogels as gradgels, where $p > q$ on the side facing hydrophilic glass and *vice versa* (Fig. 1a–b).

Before polymerization begins, the system exhibits Fickian diffusion behavior, where DMAPS aggregates near the hydrophilic surface and MAA near the hydrophobic surface. This is driven by the "like-dissolves-like" principle, where monomers preferentially migrate to substrates with matching polarity and surface tension, forming enriched layers at each interface (referred to hereafter as *Phil* and *Phob*, respectively). The monomer flux minimizes the system's free energy by preferentially partitioning monomers adjacent to surfaces with which they exhibit higher compatibility. This aligns with wetting-induced phase separation in antisymmetrically confined binary mixtures, where short-range wall–monomer interactions dominate over bulk mixing entropy.[50] In our system, no significant compositional gradient develops in the bulk cross-section because the solution rapidly transforms into a gel due to accelerated polymerization, which is facilitated by cooperative hydrogen bonding and electrostatic interactions.[44] The fast gelation kinetically traps monomers in the bulk, preventing large-scale migration. Therefore, only monomers near the surfaces diffuse efficiently before gelation occurs. It should be noted that several factors may contribute to this issue in these systems, including the electrostatic and hydrogen bonding interactions among monomer segments and the presence of CNCs. The high surface area and abundance of functional groups (*e.g.*, sulfate half esters and OH) on the CNCs can significantly impede efficient partitioning. Thus, exploring the potentially more efficient use of this shape-change programming technique on different material systems warrants further studies. The thermodynamic stability of the bulk solution in our system, far from the glass substrates that preferentially interact with DMAPS or MAA, is described by the classical Flory–Huggins miscibility framework. The bulk remains fully miscible, with χ values close to zero for all component interactions, as estimated from the Flory–Huggins relation $X = \frac{\nu}{RT}(\delta_{\text{Solvent}} - \delta_{\text{Solute}})^2$ (Table S2 and S3). The solubility parameters were calculated from the group contribution method described elsewhere.[51] We note, however, that the solubility parameters for DMAPS are approximate, since conventional group-contribution methods do not fully capture the strong coulombic interactions and solvent structuring associated with zwitterionic moieties. Thus, these values should be interpreted only as qualitative indicators of bulk miscibility rather than precise descriptors of interfacial behaviour. Despite this bulk miscibility, we hypothesize the presence of a wetting transition near the substrates, where short-ranged substrate–monomer interactions generate a localized composition gradient. In such interfacial regions, differences in interfacial tension and monomer–surface interaction energies govern the onset of stratification, consistent with theoretical treatments of self-stratifying systems.[50,52] In our case, zwitterionic DMAPS tends to lower the interfacial tension with hydrophilic glass surfaces, while the less hydrophilic MAA interacts weakly, leading to preferential enrichment of one monomer over the other near the wall. This interfacial-driven segregation results in an effective χ parameter near the substrate that differs from the bulk, controlled by surface energies and substrate-mediated phase separation. In such a design, the variation of MAA content across the hydrogel thickness produces substantial differential swelling in gradgels, where the stiffer, MAA-rich side swells more under pH > p*K*a conditions compared to the softer DMAPS-rich side, leading to local bending deformations (Fig. 2d, e and 3b). Spatial control over the surface energy of the confining glass slides can be leveraged to program the shape-change of hydrogels to more intricate profiles (Fig. 1b). Then we can employ self-healing, *via* a cut-and-paste technique, to combine monolithic gradgels into a heterolithic structure with complex deformation (Fig. 1c).

Single-domain gradgels

To verify the existence of a chemical gradient across the thickness, we measured elemental composition on the opposite sides of our gradgels using Energy Dispersive X-ray (EDX) analysis

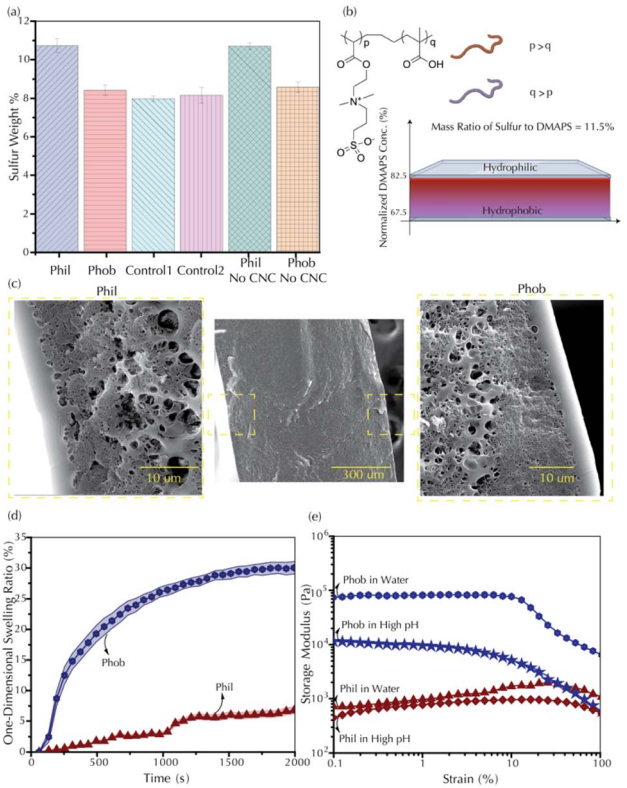

Fig. 2 Investigation of the elemental composition of gradgel. (a) Sulfur content of the samples obtained from elemental analysis of the opposite sides of the gradgel, control hydrogel, and gradgel with no added CNC. Average values are reported from three samples. (b) Schematic representation of the gradient in DMAPS concentration across the thickness of gradgel using sulfur as the characteristic element. (c) SEM image of the thickness of the gradgels showing different structural properties of the gradgel in proximity to the hydrophilic and hydrophobic walls (*phil* and *phob*, respectively). (d) Swelling-induced strain of hydrogels with composition to *phil* and *phob* layers in a high pH environment. (e) Mechanical properties of the *phil* and *phob* layers in water and in a high pH environment.

(Fig. 2a and S3-4). To quantitatively analyze the chemical composition, the intensity of the X-rays detected at energy levels corresponding to different elements (Fig. 2a) was measured. Sulfur was used as a characteristic element to estimate the mass concentration of DMAPS on each side of the gradgel, as it is exclusively present in the chemical structure of DMAPS. The mass ratio of sulfur differs by ~2.5% across the sample thickness. Using the molecular weights of DMAPS and sulfur, it is calculated that sulfur constitutes 11.5% of the mass of a DMAPS molecule. A 2.5% difference in the mass concentration of sulfur corresponds to approximately a 20% difference in the mass concentration of DMAPS on the opposite sides of the gradgel, confirming the presence of a gradient in the elemental composition across the thickness of the gradgel (Fig. 2b). EDX analysis was also performed on control samples prepared between two unmodified glass slides, as well as on gradgels with no added CNC. The results show only a negligible difference in sulfur content between the two sides of the control sample, confirming that substrate modification is essential for driving monomer migration and separation. Additionally, for gradgels prepared without CNC, the difference in sulfur concentration is comparable to that observed in regular gradgels containing 2 wt% CNC, indicating that the presence of CNC, despite its large size and amphiphilic nature, does not hinder monomer separation (Fig. 2a). It should be noted that the sulfur content of sulfuric acid-modified CNCs was assumed to be negligible, as the mass ratio of CNC to DMAPS is 1 : 27 in our formulation. The sulfur content near the hydrogel edges exposed to air and plastic spacers is lower than that in the central regions of the sample and shows only a marginal difference between the hydrophilic and hydrophobic sides in those areas (Fig. S5). To consistently eliminate the influence of hydrophobic spacers and trapped air on component phase separation, all samples used in this study were taken from the central region of the hydrogels. To further confirm the compositional gradient, we also conducted X-ray photoelectron spectroscopy (XPS) analysis on the gradgel and a non-gradient control sample. The results, which align with our EDX findings, are presented in Fig. S6 and S7 of the SI. While the difference in elemental weight percentages is lower than the EDX readings, this is expected as XPS measures only the top 10 nm of the sample's thickness, whereas EDX analyzes a depth of 1–2 μm. The difference in readings is due to the smaller sampling volume and the increased sensitivity of XPS to surface contamination.

The presence of a compositional gradient was also confirmed by SEM images, which revealed distinct structural differences across the gradgel's thickness. As previously discussed, the hydrogel remains miscible in the bulk, evidenced by the uniform structure in the middle section far from the surfaces (Fig. S8). The bulk region exhibits a uniform porous structure, contrasting with the less-porous, dense structure near the edges that were in contact with the preferentially attractive glass walls (Fig. 2c). These boundary layers, *i.e.*, *phil* and *phob* layers, constitute small portions of the sample's thickness (~35 μm for the *phil* layer and ~20 μm for the *phob* layer). Additionally, the pore morphology in the bulk regions adjacent to the *phil* and *phob* layers differs in size. Larger pores appear near the *phil* layer, while smaller pores are found near the *phob* layer. This further confirms the preferential monomer segregation in our antisymmetric hydrogel film, since DMAPS tends to form softer gels with looser hydrogel networks, whereas MAA forms stiffer gels with denser networks, as observed in the SEM images.

As mentioned before, the anisotropic distribution of components across the gradgel's thickness induces out-of-plane deformations in the form of bending for a gradgel cantilever. The shape change in gradgels occurs very fast, thanks to their monolithic structure. However, this rapid deformation is followed by fast relaxation. The *Phob* side of the gradgel is initially stiffer and swells more than the *Phil* side, which is softer and less prone to swelling (Fig. 2d and e). This contrast induces a large and rapid bending deformation in the film over time; however, the *Phob* side gradually absorbs more water at high pH and softens, reducing its ability to maintain the bent structure. As a result, the film relaxes as the mechanical imbalance diminishes. To address this issue, we added cellulose

nanocrystals (CNCs) to the hydrogel formulation as nanofillers. CNCs are one-dimensional nanoparticles with a large surface area. They possess an abundance of hydroxyl groups on their surface, forming hydrogen bonds with water molecules and neighboring CNCs.[53] During shape-change, the CNC-based non-covalent interactions in the hydrogel network preserve local deformation, delaying relaxation by postponing the onset of the quasi-equilibrium state (Fig. 3b).

To achieve an optimized bending behavior at a high pH, we changed the composition of gradgel cantilevers with an aspect ratio of 1 : 10 (width-to-length) and tested two samples with DMAPS : MAA weight ratios of 1 : 2 and 3 : 1. The results are summarized in Table S1. Significant bending was observed for the 3 : 1 sample, while the 1 : 2 sample showed minimal bending (Video S1 and 2). In the 1 : 2 formulation, the gradient of MAA concentration across the thickness of the sample is likely less pronounced compared to the 3 : 1 formulation. This can be attributed to reduced competition among the MAA molecules to reach the hydrophobic side of the cell, as MAA is the dominant monomer in the precursor. In this case, upon exposure to a high pH, the sample swells almost isotropically across its thickness.

The effect of changing CNC concentration on bending was investigated by preparing gradgels containing 1, 2, and 3 wt% CNC in the aqueous phase of the precursor. The presence of CNCs within the hydrogel structure was confirmed through Fourier Transform Infrared (FTIR) spectroscopy (Fig. S9). We observed a non-monotonic relationship between CNC concentration and bending, with samples containing 1 and 3 wt% CNC showing minimal bending, while the sample with 2 wt% CNC showed significant bending (Video S1, S3 and S4). We attribute this behavior to the optimal balance between differential swelling and mechanical properties. While the compositional gradient across the hydrogel's thickness drives the differential swelling, the degree of bending is also dependent on the material's flexibility. The reason for this behavior is rooted in the microstructure of the CNC-hydrogel composite. At 1 wt% CNC, the low concentration and high dispersibility of the CNCs likely facilitate intermolecular interactions that stiffen the network.[54] Similarly, at 3 wt% CNC, a percolation effect is observed, where the higher concentration of CNCs leads to the formation of a rigid, stiff network.[55] In contrast, the sample with 2 wt% CNC is softer, offering less mechanical resistance to the swelling force and enabling a larger bending deformation. This indicates that at this concentration, the CNCs are optimally dispersed to provide flexibility without compromising structural integrity. The rheological properties of the individual layers confirm this explanation, showing that the 2 wt% CNC sample is softer than those containing 1 wt% and 3 wt% CNC (Fig. S10). Additionally, the differential pH-induced strain across the thickness of gradgels is maintained even after the inclusion of CNCs (Fig. 2e). Therefore, the sample with 2 wt% CNC is soft and yet imposes less pH-induced strain on gradgel, creating sufficient anisotropy for bending deformation and postponing the onset of the quasi-equilibrium state by preserving local deformation through intermolecular interactions, as discussed in the System Concept. SEM images from the samples with different CNC concentrations indicate that the samples containing 1 wt% and 3 wt% CNC, show more compact microstructures compared to the sample with 2 wt% CNC, which supports the systematic mechanical studies (Fig. S11).

The effect of sample thickness on bending was studied by preparing gradgels with thicknesses of 125, 250, 500, and 750 μm (Video S1, S5–7). For thinner samples (125 and 250 mm), relaxation occurred very fast, likely due to the thin *phil* side swelling quickly, accelerating the onset of quasi-equilibrium state and relaxation. As the sample thickness increases (500 and 750 mm), the DMAPS-rich side also becomes thicker, reducing its swelling rate, and delaying the onset of the quasi-equilibrium state and relaxation.

In addition to sample thickness, the area of the cell during the separation step of preparing the sample is an important parameter influencing bending behavior. As shown in Table S1, when polymerized in a smaller cell, the gradgel cantilever shows more significant bending. This is likely due to a more planar uniformity of component separation within smaller areas. As the cell size increases, the monomers may have a larger range of motion or diffusion, leading to less uniform component separation and reduced reproducibility of bending behavior. Silanization in both gas and liquid phases was tested to make glass slides hydrophobic (see materials and methods section). Liquid-phase silanization proved more effective in inducing bending behavior in gradgel cantilevers. This can be attributed to the effect of the liquid medium in creating a more uniform surface modification, which enhances the hydrophobic interactions with the hydrogel components. As a result of enhanced hydrophobic interactions, component separation improves, leading to more pronounced and reproducible bending behavior.

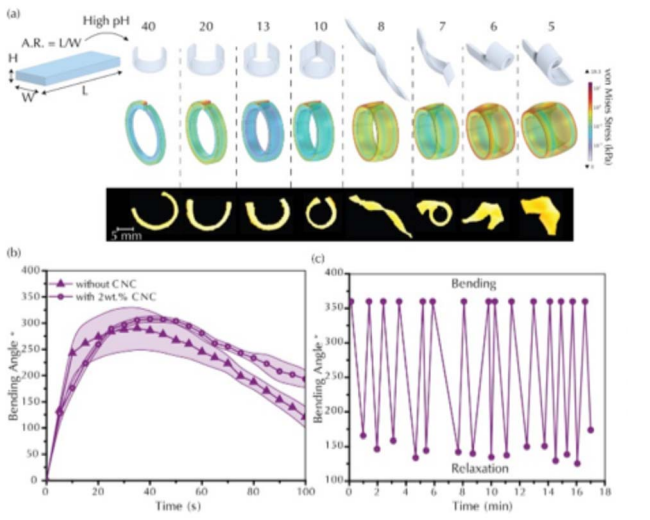

Fig. 3 Shape-change programming through sample geometry. (a) Deformation mode as a function of the aspect ratio of the gradgel cantilever. (b) Bending angle of a cantilever (with and without CNC) with a 1 : 10 (width to length) aspect ratio over time. (c) Repeatability of the bending deformation by an alternative change of the pH of the environment from basic to acidic.

Cutting the gradgel cantilevers to different aspect ratios was utilized as a tool to program their shape-change behavior. In addition to the biased gradient of chemical composition across the thickness, the mass transport occurs gradually during swelling. That is, peripheral regions exposed to the buffer swell more rapidly than central regions, leading to anisotropic and transient modes of deformation such as twisting or buckling. This effect diminishes over time as water permeates the entire sample. Narrower samples, indeed, do not demonstrate buckling and twisting. As shown in Fig. 3a, there is a correlation between the aspect ratio of the gradgel cantilever and its deformation mode upon exposure to a high pH environment. Narrow samples with a higher length-to-width ratio show pure bending, while wider samples with a lower length-to-width ratio twist after exposure to a high pH environment (Video S8). To isolate the effect of the chemical gradient, we prepared control samples using the same formulation in between unmodified glass slides. These uniform hydrogels showed no deformation when exposed to high pH (Video S9), confirming the critical role of the compositional gradient in our shape-change method.

In principle, the deformation mechanics of our monolithic hydrogel cantilevers resemble those of bilayer structures, following Timoshenko's bimetallic theory.[56] This theory correlates deformation to the geometric parameters and material properties of each layer, as well as the ratio between the bilayer's length and width. To describe the deformations of hydrogels at any point on their structure, the principal curvatures (k_1 and k_2) can be used to calculate the mean ($H = \frac{k_1 + k_2}{2}$) and Gaussian ($K = k_1.k_2$) curvature. The principal curvatures depend on the extent of differential swelling of the hydrogel across the thickness and across the plane. Hydrogels with differential swelling across the thickness bend ($H \neq 0$ and $K = 0$), while hydrogels with bidirectional differential swelling (across the thickness and the plane) buckle ($H \neq 0$ and $K \neq 0$) to minimize their elastic free energy.[26,27,57] In our geometry-dependent shape-change programming strategy, narrower samples exhibit a negligible gradient of chemical composition and water mass transport across the plane due to their small size, resulting in only bending toward the DMAPS-rich side of the sample. As the sample width increases, the gradient of chemical composition and water mass transport across the plane becomes more pronounced, leading to bending and twisting and the emergence of both mean and Gaussian curvatures. The observed deformation modes align with the simulation results presented in Fig. 3a. Using finite-element modeling, macroscopic continuum elastic behavior of bilayer beams is simulated, revealing the onset of bending and/or buckling. As indicated by the simulation results, decreasing the aspect ratio increases the internal von Mises stress, which makes the structure collapse or buckle, which manifests in experiments by twisting. Note that our finite element model can be strengthened by including the kinetics of swelling in-plane to capture the more pronounced transient nature of mass transport in wider samples. This is a subject of future study.

Additionally, the shape-change in our gradgel cantilevers occurs very fast, thanks to the monolithic structure of the samples. As shown in Fig. 3b, a gradgel cantilever with an aspect ratio of 1 : 10 for width to length bends around 300° in less than 30 seconds (Video S1). This rapid shape-change is repeatable for at least 15 cycles through alternating exposure to media with high and low pH values, respectively (Fig. 3c and Video S9). Fig. 3b indicates the role of CNC in preserving the deformation. As can be seen in the graph, the sample without CNC deforms faster (the slope of the graph is steeper) compared to the sample containing CNC. The sample without CNC also relaxes faster, and its final residual deformation is only about 100°, meaning it barely drifts. The sample containing CNC, although initially bends more slowly (less steep slope), holds the deformation longer, as indicated by the more significant drift (about 200°). We should note that the addition of CNC potentially interferes with monomer stratification, since CNC has a high surface area and abundance of functional groups. However, there is a trade-off here, and the major role of CNC is to preserve the deformation through its hydrogen bonding with water molecules, thereby preserving local deformation. Additionally, the maximum theoretical work density is about 3 kJ m^{-3}, which is estimated from the difference between the area under the stress–strain plots for the gradgel swelled in water and high pH (Fig. S12).

Multi-domain gradgels

In addition to encoding simple shape-changes through gradgel geometry, patterning glass slides with domains of different hydrophobicity was used to program more complex shape-changes in the monolithic hydrogels. In this method, a cell was formed using glass slides with domains of hydrophilic and hydrophobic modifications, creating an in-plane domain-specific gradient of chemical composition in gradgels polymerized within these cells (Fig. 4ai–iii). Depending on the hydrophobic patterns on the glass slide, chemical gradients occur in the same or opposite directions across different domains of the gradgels. Upon exposure to a high pH environment, gradgels containing two domains of opposing chemical gradient deform to an S-shape construct. Gradgels containing two domains of similar chemical gradient separated by a neutral area deform to an M-shape construct. All these deformation behaviors are verified by the simulations (Fig. 4b–di and ii, Video S11 and 12). The M-shaped deformation can be modified by decreasing the width of the cantilever to result in two separate coil deformations at two ends (Fig. 4a–diii). In such a high aspect ratio beam, the more pronounced bending deformation causes the sample to bend rapidly at both ends, which drags the unmodified middle part to stretch and forms a two-sided bending deformation (Fig. 4a–diii, Video S13).

Thanks to the self-healing properties of the hydrogel system, a cut-and-paste technique was used to make a heterolithic hydrogel construct resembling an octopus. Using the geometry-based shape-change programming technique, eight gradgel cantilevers with different shape-change profiles were created, like those reported in Fig. 3a. To assemble such an octopus-like structure, cantilevers were attached to a circular body made of the same hydrogel but with no gradient to prevent anisotropic

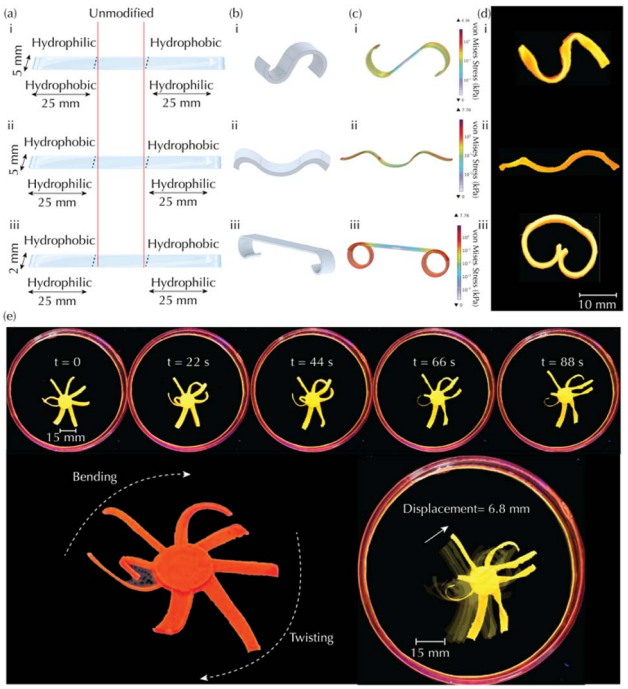

Fig. 4 Shape-change programming through glass slide patterning. (a) Schematic representation of the component distribution in gradgels made by glass slide patterning. (b) Schematic representation of the shape-change mode of the patterned gradgels after exposure to the high pH environment. (c) Simulation of the shape-change mode of the patterned gradgels upon exposure to a high pH environment. (d) Programmed shape-change of the patterned gradgels upon exposure to the high pH environment. (e) Rapid forward movement of an octopus hydrogel composed of gradgel legs with different aspect ratios.

swelling of the central body. The pieces of hydrogel were collaged together by placing the cantilevers in contact with the central body and applying mild pressure using a glass slide placed on top of the construct for 30 minutes. After this period, the construct was placed in a high pH environment to investigate its collective shape-change behavior. As shown in Fig. 4e, upon exposure to a high pH environment, the narrower legs bent while the wider legs twisted, causing the octopus hydrogel to move forward rapidly, considering the overall size of the construct (Video S14).

Conclusions

In this work, we reported a simple shape-change programming technique for controlling the deformation profile of stimuli-responsive hydrogels at multilevel complexity. The technique is based on facile surface modification methods to tune the affinity of glass slides in contact with the hydrogel precursor during sample preparation. The hydrogel system studied for shape-change programming contains MAA and DMAPS, two monomers with significantly different polarities, physicochemical, and mechanical properties. MAA is a less hydrophilic and pH-responsive monomer that provides relatively stiff characteristics to the hydrogel network containing it. DMAPS is a super-hydrophilic zwitterionic monomer that renders softness and self-healing properties to the hydrogel network thanks to its intrinsic electrostatic interactions. Slight chemical cross-linking, along with the addition of CNC as a swelling regulator, ensures the mechanical integrity of the hydrogel. Upon contact of the hydrogel precursor with the surface-modified glass slides arranged into a cell, attractive forces between hydrogel components and glass slides with similar hydrophilicity drive component separation across the sample's thickness, *i.e.*, the hydrogel composition is rich in MAA near the hydrophobic side of the cell and rich in DMAPS near the hydrophilic side. After photopolymerization, the gradient in chemical composition creates gradients in physicochemical and mechanical properties across the thickness. Therefore, exposure of polymerized hydrogels to a high environmental pH induces differential swelling across the thickness, where the extent of swelling is directly proportional to the MAA concentration. This, combined with the mechanical superiority of MAA, forms a curvature toward the DMAPS-rich side. This deformation occurs very fast, in the order of a few seconds.

Changing the aspect ratio (length-to-width) of the samples was used as a tool to program the shape-change profile, where increasing the aspect ratio leads to bending deformation, while decreasing the aspect ratio leads to twisting deformation. This change in deformation profile is due to the change in component separation mode, from monodirectional (across the thickness) separation in narrower samples to bidirectional (across the thickness and the plane) separation in wider samples. Expanding on our shape-change programming technique, we used glass slide patterning to program local component separation in our hydrogel samples to create more complex deformations. Using this technique, we achieved more complex shape changes, such as S-shape, M-shape, and coil deformations, in our monolithic hydrogels. Additionally, the self-healing properties of the hydrogel system allow for a cut-and-paste technique to achieve a simple robotic function for an octopus hydrogel composed of eight rectangular legs with different aspect ratios and shape-change profiles attached to a circular hydrogel body. Upon exposure to a high pH environment, the simultaneous bending of narrower legs and twisting of wider legs results in the rapid forward movement of the octopus hydrogel.

Overall, our shape-change programming strategy is a simple yet versatile technique applicable not only to other hydrogel systems but also to any soft material system containing components with different polarities that could undergo a controlled change in physical state, such as from liquid to solid, during preparation. While this work serves as a foundational proof-of-concept, we believe it lays the groundwork for future research to validate its broad applicability. Future studies will focus on investigating the dependency on specific monomer pairs, exploring substrate modifications, and demonstrating more sophisticated and scalable deformations. Our introduced material system is particularly well-suited for small-scale medical robots, with potential application in environments with built-in pH variations, such as the gastrointestinal or reproductive tracts. In these scenarios, the material's inherent pH responsiveness eliminates the need for external

acid or base dosing, enabling actuation without the need for external control. Beyond this specific material system, the core contribution of our work is the novel and simple fabrication method for shape-change programming. By relying on material gradients rather than complex structural anisotropy, this technique offers a versatile approach that can be applied to other stimuli-responsive material systems. We believe this concept provides a powerful new tool for designing soft robotic actuators and other smart devices for a wide range of real-world applications. Our presented method for shape-change programming of binary hydrogel systems is straightforward and results in rapid deformations. However, it crucially depends on the wetting behavior of the glass substrates after surface treatment, which may be subject to batch-to-batch variability. Utilization of advanced anti-stiction coating tools and techniques prevalent in microelectromechanical systems (MEMEs) in conjunction with lithography-based surface masking and patterning is a potential way to dramatically enhance the reproducibility and scalability of our strategy. Future work will also focus on realizing more sophisticated robotic functions, such as controlled capture, transport, and release of cargo, for hydrogel constructs using the presented shape-change programming technique. Achieving such robotic functions represents a step toward envisioning a future generation of biomedical, surgical, and therapeutic soft robots based on our hydrogel system.

Experimental section

Materials

3-Dimethyl (methacryloyloxyethyl) ammonium propanesulfonate (DMAPS, 95%), 2-Hydroxy-2-methylpropiophenone (97%), Hydrochloric acid (HCl, 37%), Sodium hydroxide pellets (NaOH, ≥ 97%), *N*,*N*′-Methylenebis(acrylamide) (BIS, 99%), Trichloro(1*H*,1*H*,2*H*,2*H*-perfluorooctyl)silane (97%), Toluene (>99.9%), Rhodamine B (≥95%),and Methacrylic acid (MAA, 99%) were purchased from Sigma-Aldrich Co., Canada. Cellulose nanocrystal (CNC, ≥ 94%) was acquired from CelluForce Inc., Canada. Deionized water (DI water, > 16 MΩ cm resistivity) was used in all of the experiments. All the chemicals were used without further purification.

Hydrophobic glass slide modification

Gas phase silanization. Five droplets of Trichloro(1*H*,1*H*,2*H*,2*H*-perfluorooctyl)silane were poured into a small vial in a desiccator connected to a vacuum pump. The glass slides were cleaned with acetone, isopropanol, and DI water and were put in the desiccator and kept under vacuum for two hours.

Liquid phase silanization. A 5 wt% solution of Trichloro(1*H*,1*H*,2*H*,2*H*-perfluorooctyl)silane was made in toluene and clean glass slides were submerged in the solution for two hours under the fume hood.

Hydrophilic glass slide modification. Clean glass slides were put into the chamber of a UV-Ozone plasma cleaner and treated for 30 minutes at room temperature.

Glass slide patterning. A 5 wt% solution of trichloro(1*H*,1*H*,2*H*,2*H*-perfluorooctyl)silane in toluene was prepared, and clean glass slides were submerged in the solution for two hours under a fume hood. For experiments with patterned glass slides, the glass slides were clamped vertically, and the desired portion of each slide was submerged in the beaker containing the solution. The remaining parts of the glass slide were covered with electrical tape to prevent hydrophobic modification in those areas. For example, one-third of a glass slide with dimensions of 20 mm × 25 mm was modified using this method, while the remaining two-thirds were kept taped to prevent hydrophobic surface modification. After thorough cleaning, we taped the remaining two-thirds of the glass slide, including the silanized portion, and performed a UV-Ozone plasma treatment on the exposed one-third to render it super hydrophilic. The middle one-third of the glass slide was left unmodified to create a buffer zone, preventing baffled component separation at the interface between the hydrophobic and hydrophilic regions. In another experiment, the glass slides were patterned to create two identical surface modifications at their ends. For one glass slide, after taping two-thirds of the slide that had been silanized at one end, the exposed end was soaked in the silane solution instead of undergoing UV-Ozone treatment, rendering the other end hydrophobic as well. For the other glass slide, UV-Ozone plasma treatment was applied to both ends, creating two hydrophilic regions. The middle one-third of the glass slide was also left unmodified in this experiment, creating a buffer zone for component separation. The two glass slides were then arranged into a cell.

Hydrogel preparation. 5 g of CNC suspension with different concentrations was added to a mixture of DMAPS and MAA with different weight ratios. The total monomer concentration was kept at 50 wt%. 30 mg BIS (monomer : BIS weight ratio 1000 : 6), and 30 mg 2-Hydroxy-2 methylpropiophenone (monomer : initiator weight ratio 1000 : 6) were added to the mixture, followed by vortex mixing and bath sonication. The mixture was purged with nitrogen for 10 minutes before storing in the fridge. For sample preparation, the hydrogel precursor was injected into a cell prepared by two glass slides separated by two strips of spacers with known thicknesses. Hydrophobic/hydrophilic modification was performed on the glass slides before injecting the precursor. The glass slides were arranged in a way that the hydrophobic part of one glass slide faced the hydrophilic part of the other glass slide. After the injection of the hydrogel precursor, the cell rested for an hour to allow the monomer separation imposed by different hydroaffinities of the monomers. The UV-polymerization was conducted in a container purged with nitrogen. Each side of the cell was exposed to the UV light of wavelength 365 nm for 30 min.

Preparation of "phil" and "phob" layers. The compositions of the individual "phil" and "phob" layers were estimated by analyzing the as-prepared anisotropic hydrogels. Using EDX analysis, a DMAPS concentration gradient of 20% was observed across the thickness of the sample. Assuming this gradient occurs linearly, we approximated the compositions of the "phil" and "phob" layers to represent the DMAPS concentration at the

two opposing surfaces. With a total monomer mass of 5 g and a total DMAPS mass of 3.75 g in the original formulation, the DMAPS content was calculated to be 10% less and 10% more, respectively, in the "phob" and "phil" layers compared to the average DMAPS concentration in the sample. This led to the preparation of simulated "phob" and "phil" formulations with DMAPS to total monomer mass ratios of 3.375/5 and 4.125/5, respectively. These samples were then subjected to swelling and mechanical property tests to characterize the individual layers.

Characterization

ImageJ was used to measure the degree of bending/relaxation by measuring the angle between a vertical tangent applied to one edge of the hydrogel and a vector connecting two edges after bending/relaxation, which was triggered by increasing the pH of the hydrogel environment. Swelling tests were conducted by immersing polymerized hydrogels in deionized water overnight. The equilibrated gels were sectioned into uniform 5 mm × 5 mm specimens and transferred to a polystyrene Petri dish containing an aqueous NaOH solution (pH ~12) to initiate pH-responsive swelling. To enable fluorescence tracking, Rhodamine B-labeled hydrogels were irradiated with a 365 nm UV light source (ENF 280C), and video recording was performed using a Nikon D3600 digital camera. The experimental setup, including the Petri dish, UV source, and camera, was enclosed within a light-absorbing enclosure to minimize ambient light interference and enhance optical contrast. Acquired video data were digitally processed and temporally segmented into frames at 1-minute intervals. Each frame was analyzed using a custom ImageJ macro script (Fiji distribution) to quantify the projected area of the hydrogel specimens. Due to the isotropic swelling behavior of the hydrogel samples, dimensional changes were assumed equivalent across all axes. Thus, the square root of the projected area was computed to estimate the mean linear expansion during swelling. The pH-induced strain of the samples was measure by dividing the change in the length over the initial length of the sample. The degree of monomer separation was quantified by EDX characterization and the morphology of the samples was analyzed by SEM imaging performed on a FEI Quanta Feg 250 ESEM (with EDX). The samples were cut into 5 mm' 5 mm squares and freeze dried in a Lab-Conco 4 L freeze dryer for 24 hours before conducting the experiment. Two opposite sides of the samples were analyzed to determine the elemental composition of each side. The mechanical properties of the hydrogels were investigated using a rheometer (Discovery HR20, TA Instruments) equipped with a 20 mm parallel plate geometry featuring a 0.75 mm gap. Strain sweep ranging from 0.1% to 100% was carried out at a consistent frequency of 1 Hz to identify the shear modulus of the samples.

Simulation

The mechanical deformation of gradgels was modeled using finite element software COMSOL Multiphysics 6.3. The gradgels were modeled as isotropic bilayer beams with neo-Hookean hyperelastic models to account for the large mechanical deformation. The composite cross-section thickness of the gradgel beams is constituted of a 150μm-thick Phob layer and a 600μm-thick Phil layer. The elastic properties of the beams were estimated from the experimentally measured storage modulus (G'), and the measured strain behavior was given as an input for the incremental deformation of the bilayer beam. Since the deformation of gradgels occurred in a reduced environment, the storage modulus of the Phob layer was estimated to be around 10 kPa at high pH. For simulations shown in Fig. 3a, the mechanical boundary conditions were set as cantilever beams having a fixed displacement at one edge. For simulations shown in Fig. 4c, a two-edge fixed displacement was set as a boundary condition.

Author contributions

N. B. contributed to conceptualization, data curation, formal analysis, investigation, methodology design, validation, visualization, project administration, and writing of the original draft, as well as review and editing. M. A., E. H., and M. B. contributed to data curation and visualization. A. A. performed simulations, contributed to validation, and supported the writing of the original draft. N. S. supported software utilization. H. S. contributed to conceptualization, funding acquisition, project administration, supervision, validation, and review and editing.

Conflicts of interest

There are no conflicts to declare.

Data availability

All data required for the reproduction of the results are shown in this article and its supporting information (SI). Supplementary information is available. See DOI: https://doi.org/10.1039/d5ta08956e.

Acknowledgements

This work is supported by the Natural Sciences and Engineering Research Council of Canada (NSERC).

Notes and references

1 X. P. Hao, C. Y. Li, C. W. Zhang, M. Du, Z. Ying, Q. Zheng and Z. L. Wu, *Adv. Funct. Mater.*, 2021, **31**, 1–10.
2 S. Y. Zheng, Y. Shen, F. Zhu, J. Yin, J. Qian, J. Fu, Z. L. Wu and Q. Zheng, *Adv. Funct. Mater.*, 2018, **28**, 1–8.
3 Y. S. Kim, M. Liu, Y. Ishida, Y. Ebina, M. Osada, T. Sasaki, T. Hikima, M. Takata and T. Aida, *Nat. Mater.*, 2015, **14**, 1002–1007.
4 B. J. Nelson, I. K. Kaliakatsos and J. J. Abbott, *Annu. Rev. Biomed. Eng.*, 2010, **12**, 55–85.
5 M. Li, A. Pal, A. Aghakhani, A. Pena-Francesch and M. Sitti, *Nat. Rev. Mater.*, 2021, **7**, 235–249.

6 S. Palagi and P. Fischer, *Nat. Rev. Mater.*, 2018, **3**, 113–124.
7 M. Sitti, *Nature*, 2009, **458**, 1121–1122.
8 G.-Z. Yang, J. Bellingham, P. E. Dupont, P. Fischer, L. Floridi, R. Full, N. Jacobstein, V. Kumar, M. McNutt, R. Merrifield, B. J. Nelson, B. Scassellati, M. Taddeo, R. Taylor, M. Veloso, Z. L. Wang and R. Wood, *Sci. Robot.*, 2018, **3**, eaar7650.
9 P. Fischer, B. J. Nelson and G.-Z. Yang, *Sci. Robot.*, 2018, **3**, eaau0448.
10 S. Zhang, X. Ke, Q. Jiang, Z. Chai, Z. Wu and H. Ding, *Adv. Mater.*, 2022, **34**, 2200671.
11 C. A. Aubin, B. Gorissen, E. Milana, P. R. Buskohl, N. Lazarus, G. A. Slipher, C. Keplinger, J. Bongard, F. Iida, J. A. Lewis and R. F. Shepherd, *Nature*, 2022, **602**, 393–402.
12 P. Xue, H. K. Bisoyi, Y. Chen, H. Zeng, J. Yang, X. Yang, P. Lv, X. Zhang, A. Priimagi, L. Wang, X. Xu and Q. Li, *Angew. Chem., Int. Ed.*, 2021, **60**, 3390–3396.
13 T. Hiratani, O. Kose, W. Y. Hamad and M. J. MacLachlan, *Mater. Horiz.*, 2018, **5**, 1076–1081.
14 O. Kose, C. E. Boott, W. Y. Hamad and M. J. MacLachlan, *Macromolecules*, 2019, **52**, 5317–5324.
15 K. Liu, Y. Zhang, H. Cao, H. Liu, Y. Geng, W. Yuan, J. Zhou, Z. L. Wu, G. Shan, Y. Bao, Q. Zhao, T. Xie and P. Pan, *Adv. Mater.*, 2020, **32**, 1–7.
16 M. Chau, K. J. De France, B. Kopera, V. R. Machado, S. Rosenfeldt, L. Reyes, K. J. W. Chan, S. Förster, E. D. Cranston and T. Hoare, *Chem. Mater.*, 2016, **28**, 3406–3415.
17 I. Tokarev and S. Minko, *Soft Matter*, 2009, **5**, 511–524.
18 J. L. Drury and D. J. Mooney, *Biomaterials*, 2003, **24**, 4337–4351.
19 Y. Qiu and K. Park, *Adv. Drug Deliv. Rev.*, 2001, **53**, 321–339.
20 S. Ahn, R. M. Kasi, S.-C. Kim, N. Sharma and Y. Zhou, *Soft Matter.*, 2008, **4**, 1151–1157.
21 Z. Shen, F. Chen, X. Zhu, K.-T. T. Yong and G. Gu, *J. Mater. Chem. B*, 2020, **8**, 8972–8991.
22 O. E. Shklyaev and A. C. Balazs, *Nat. Nanotechnol.*, 2023, 1–14.
23 A. Gevorkian, S. M. Morozova, S. Kheiri, N. Khuu, H. Chen, E. Young, N. Yan and E. Kumacheva, *Adv. Funct. Mater.*, 2021, **31**, 1–9.
24 S. J. Jeon, A. W. Hauser and R. C. Hayward, *Acc. Chem. Res.*, 2017, **50**, 161–169.
25 O. Erol, A. Pantula, W. Liu and D. H. Gracias, *Adv. Mater. Technol.*, 2019, **4**, 1900043.
26 T. van Manen, S. Janbaz and A. A. Zadpoor, *Mater. Today*, 2018, **21**, 144–163.
27 S. Janbaz, R. Hedayati and A. A. Zadpoor, *Mater. Horiz.*, 2016, **3**, 536–547.
28 Y. Chang, A. Venault, C.-W. W. Huang, J. Zheng, A. Chinnathambi, S. A. Alharbi, Y. Cheng, Y. Chang, Y. Chang, A. Venault, C.-W. W. Huang, J. Zheng, A. Chinnathambi, S. A. Alharbi and Y. Cheng, *Int. J. Polym. Mater. Polym. Biomater.*, 2016, **65**, 65–74.
29 H. Arslan, A. Nojoomi, J. Jeon and K. Yum, *Advanced Science*, 2019, **6**, 1800703.
30 C. Ma, X. Le, X. Tang, J. He, P. Xiao, J. Zheng, H. Xiao, W. Lu, J. Zhang, Y. Huang and T. Chen, *Adv. Funct. Mater.*, 2016, **26**, 8670–8676.
31 A. Nojoomi, J. Jeon and K. Yum, *Nat. Commun.*, 2021, **12**, 603.
32 J.-H. Na, N. P. Bende, J. Bae, C. D. Santangelo and R. C. Hayward, *Soft Matter*, 2016, **12**, 4985–4990.
33 M. Chen, J. Zhu, G. Qi, C. He and H. Wang, *Mater. Lett.*, 2012, **89**, 104–107.
34 R. Nasseri, N. Bouzari, J. Huang, H. Golzar, S. Jankhani, X. Tang, T. H. Mekonnen, A. Aghakhani and H. Shahsavan, *Nat. Commun.*, 2023, **14**, 6108.
35 Y. Guo, H. Shahsavan and M. Sitti, *Adv. Mater.*, 2020, **32**, 1–10.
36 J. Zhang, Z. Ren, W. Hu, R. H. Soon, I. C. Yasa, Z. Liu and M. Sitti, *Sci. Robot.*, 2021, **6**, eabf0112.
37 Y. Guo, J. Zhang, W. Hu, M. T. A. Khan and M. Sitti, *Nat. Commun.*, 2021, **12**, 5936.
38 M. Rafiee, R. D. Farahani and D. Therriault, *Advanced Science*, 2020, **7**, 1902307.
39 G. D. Zartman and S.-Q. Wang, *Macromolecules*, 2011, **44**, 9814–9820.
40 P. C. Lee, H. E. Park, D. C. Morse and C. W. Macosko, *J. Rheol.*, 2009, **53**, 893–915.
41 H. Zhang, K. Lamnawar, A. Maazouz and J. M. Maia, *J. Rheol.*, 2016, **60**, 1–23.
42 H. Tokuyama, M. Sasaki and S. Sakohara, *Colloids Surf., A*, 2006, **273**, 70–74.
43 I. Yu. Konotop, I. R. Nasimova, M. V Tamm, N. G. Rambidi and A. R. Khokhlov, *Soft Matter*, 2010, **6**, 1632–1634.
44 X. Peng, Y. Li, Q. Zhang, C. Shang, Q.-W. Bai and H. Wang, *Adv. Funct. Mater.*, 2016, **26**, 4491–4500.
45 S. Maeda, Y. Hara, T. Sakai, R. Yoshida and S. Hashimoto, *Adv. Mater.*, 2007, **19**, 3480–3484.
46 R. Knoesel, M. Ehrmann and J. C. Galin, *Polymer*, 1993, **34**, 1925–1932.
47 T. P. Stepanova and O. E. Philippova, *Polym. Sci., Ser. A*, 2006, **48**, 428–434.
48 N. Bouzari, R. Nasseri, J. Huang, S. Ganguly, X. Tang, T. H. Mekonnen, A. Aghakhani and H. Shahsavan, *Small Methods*, 2025, **9**, 2400812.
49 J. Zhang and N. A. Peppas, *Macromolecules*, 2000, **33**, 102–107.
50 M. Müller and K. Binder, *Int. J. Thermophys.*, 2006, **27**, 448–466.
51 E. Stefanis and C. Panayiotou, *Int. J. Thermophys.*, 2008, **29**, 568–585.
52 C. Carr and E. Wallstöm, *Prog. Org. Coat.*, 1996, **28**, 161–171.
53 J. Shojaeiarani, D. Bajwa and A. Shirzadifar, *Carbohydr. Polym.*, 2019, **216**, 247–259.
54 Y. Cao, P. Zavattieri, J. Youngblood, R. Moon and J. Weiss, *Constr. Build. Mater.*, 2016, **119**, 71–79.
55 H. J. Kim, Y. H. Choi, J. H. Jeong, H. Kim, H. S. Yang, S. Y. Hwang, J. M. Koo and Y. Eom, *Macromol. Res.*, 2021, **29**, 720–726.
56 S. Timoshenko, *J. Opt. Soc. Am.*, 1925, **11**, 233–255.
57 A. Sydney Gladman, E. A. Matsumoto, R. G. Nuzzo, L. Mahadevan and J. A. Lewis, *Nat. Mater.*, 2016, **15**, 413–418.

